Algorithm of global Gross and net primary productivity products

Rui Sun, Zhiqiang Xiao, Juanmin Wang, Anran Zhu, Mengjia Wang

The State Key Laboratory of Remote Sensing Science, Jointly Sponsored by Beijing Normal University and Institute of Remote Sensing Applications of Chinese Academy of Sciences, Beijing,China；

Beijing Engineering Research Center for Global Land Remote Sensing Products, Institute of Remote Sensing Science and Engineering, Faculty of Geographical Science, Beijing Normal University, Beijing 100875,China

1. Introduction

The vegetation productivity of terrestrial ecosystems allows quantification of the conversion of carbon dioxide (CO_2) in the atmosphere to plant biomass and reflects the ability to fix atmospheric CO_2 from vegetation, which is an important variable for estimating the global carbon budget, and it is also an important ecological indicator for estimating the Earth's carrying capacity and the sustainable development of terrestrial ecosystems. There are mainly three types of vegetation productivity models, i.e. empirical models based on the statistical relationship between vegetation productivity and climate factors (Lieth, 1975; Uchijima and Seino, 1985), process models based on the ecophysiological processes of plant growth （McGuire et al., 1996; Running and Hunt, 1993; Liu et al., 1997), and the light use efficiency (LUE) models based on absorbed photosyntheticallly active radiation (APAR) and LUE （Potter et al., 1993; Prince and Goward, 1995; Zhao and Running, 2010; Xiao et al., 2004; Yuan et al., 2007） .

The global gross primary productivity (GPP) and net primary productivity (NPP) products here were estimated from a LUE based algorithm and a long-term series of global land and terrestrial satellite (GLASS) leaf and index (LAI) and fraction of absorbed photosynthetically active radiation (FPAR) products from 1981 to 2018. The products had a spatial resolution of 0.05 degree in every 8 days. In the estimation of LUE, the effect of the fraction of diffuse solar radiation on LUE were taken into account by adding the clearness index (CI) factor.

2. Algorithm description

GPP and NPP were estimated by improved Multisource Data Synergized Quantitative-Net Primary Productivity (MuSyQ-NPP) algorithm, which is a LUE model and has been validated by Cui et al. (2016) and Yu et al. (2018). Many studies have found that the LUE of diffuse solar radiation is higher than that of direct solar radiation (Xin et al., 2016; He et al., 2013). The consideration of the effect of the fraction of diffuse solar radiation on LUE might improve the accuracy of GPP and NPP estimation, especially in cloudy areas, such as tropical evergreen broadleaf forests. Wang et al. (2020) recently compared three LUE estimate approaches and found that the parameterization approach with the clearness index (CI) could improve LUE and GPP estimation. Therefore, based on the study of Wang et al. (2020), we estimated LUE by adding the CI to improve the accuracy of GPP estimation (Figure 1).
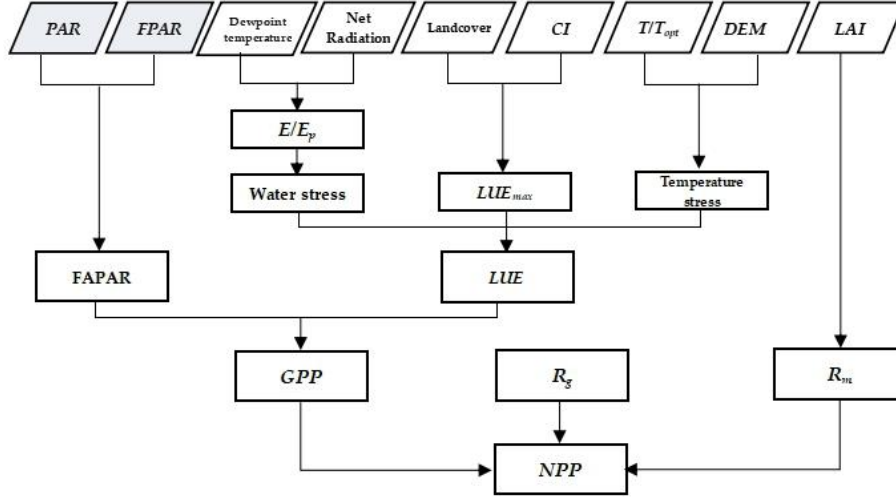
Figure 1. Diagram of GPP and NPP estimation with the improved MuSyQ-NPP algorithm

2.1 GPP estimation

GPP (gC/m²d) was estimated according to LUE and absorbed photosynthetically active radiation (APAR).

$$GPP = LUE \times FPAR \times PAR \tag{1}$$

where LUE is actual light use efficiency (gC/MJ), FPAR is the fraction of absorbed photosynthetically active radiation by vegetation, and PAR is incident photosynthetically active radiation (MJ/m²d).

LUE was calculated with a parameterization approach, in which the maximum LUE without stress was determined according to the vegetation type and clearness index (CI), and the actual LUE was estimated by multiplying the temperature stress and water stress. The CI was adopted to reflect the effect of diffuse light fraction in the incident solar radiation on LUE.

$$LUE = [LUE_{\max}^{su} \times CI + LUE_{\max}^{sh} \times (1 - CI)] \times f(W) \times f(T) \tag{2}$$

The formula in the bracket represents the maximum LUE (LUE$_{max}$), which is calculated by weighting LUE$_{max}$ for sunlit leaves (LUE_{max}^{su}, gC/MJ) and LUE$_{max}$ for shaded leaves (LUE_{max}^{sh}, gC/MJ). LUE_{max}^{su} and LUE_{max}^{sh} were simultaneously optimized by Shuffled Complex Evolution method developed at the University of Arizona (SCE-UA) optimization algorithm (Duan et al., 1992) and data from FLUXNET2015 dataset (https://fluxnet.fluxdata.org/data/). CI and (1-CI) are the weight coefficients. CI is clearness index, which represents the fraction of solar incident radiation on the surface of the earth ($SW_{surface}$, MJ/m²d) to the extraterrestrial radiation at the top of the atmosphere (SW_{top}, MJ/m²d).

$$CI = \frac{SW_{\text{surface}}}{SW_{\text{top}}} \tag{3}$$

$$SW_{top} = \frac{TD}{\pi} S_0 (\omega_0 sin\varphi sin\delta + cos\varphi cos\delta sin\omega_0) \qquad (4)$$

$$S_0 = \overline{S_0} \times (1 + 0.033 \times cos(2\pi \times \frac{day}{365}))^2 \qquad (5)$$

$SW_{surface}$ is from ERA-Interim dataset. TD represents the time period of a day, and $TD =$ 60*60*24 = 86400 seconds. $\overline{S_0}$ represents solar radiation constant, equal to 1367W/m². ω_0 is solar Horizon at Sunrise. φ is latitude. δ is solar declination.

$f(T)$ is a temperature stress factor. The growth performance of vegetation is influenced by the average temperature (T, °C) (Potter et al., 1993).

$$f(T) = \frac{1}{[1 + e^{0.2(T_{opt}-10-T)}] \times [1 + e^{0.3(-T_{opt}-10+T)}]} \qquad (6)$$

T_{opt} (°C) is the optimum growth temperature, which is average temperature when vegetation grows best. We counted the average temperature in the month when LAI reached the maximum for different vegetation types first, and then SCE-UA optimization algorithm was used to optimize the T_{opt} value for different vegetation types (Table 1).

$f(W)$ describes the water stress factor and can be obtained by the following formula:

$$f(W) = 0.5 + 0.5(E/E_p) \qquad (7)$$

where E represents the actual evapotranspiration (mm), which is calculated from a modified Penman-Monteith approach (Zhang et al., 2009) using the GLASS LAI products. E_p represents the potential evapotranspiration (mm), which is derived from the Priestley and Taylor equation (Priestley and Taylor, 1992)0. $f(W)$ is forced to be equal to 1.0 when it exceeds 1.0.

FPAR is from the GLASS FPAR product. PAR (MJ/m²d) was calculated from $SW_{surface}$ using the following formula.

$$PAR = 0.48 \times SW_{surface} \qquad (8)$$

2.2 NPP estimation

NPP (gC/m²d) is the net flow of carbon entering the plants from the atmosphere and represents the remainder after deducting the organic matter consumed by plant autotrophic respiration from GPP.

$$NPP = GPP - R_a \qquad (9)$$

where R_a (gC/m²d) is the autotrophic respiration. It can be separated into two parts, maintenance respiration R_m and growth respiration R_g, which refer to the energy necessary to maintain biomass and the energy converting assimilates into new structural plant constituents, respectively (Cui et al., 2016).

$$R_a = R_m + R_g = \sum R_{mj} + R_g \qquad (10)$$

$$R_{m,i} = M_i r_{m,i} Q_{10,i}^{(T-T_b)/10} \qquad (11)$$

Where M_i is the live biomass of plant component i, which is calculated by LAI and annual maximum LAI for each pixel. $r_{m,i}$ is maintenance respiration coefficient for component i, Q is the temperature sensitivity factor, T is the daily average temperature and T_b is the base temperature.

Growth respiration R_g was considered to be proportional to the difference between GPP and maintenance respiration R_m:

$$R_g = \gamma(GPP - R_m)$$
(12)

Where γ is the growing respiration efficient and is defined as 0.25.

2.3 Water stress factor estimation

In order to determine the water stress factor in formula (7), evapotranspiration and potential evapotranspiration were estimated. Daily actual evapotranspiration was estimated by a modified Penman-Monteith approach with biome-specific canopy conductance (Zhang et al., 2009). Evapotranspiration was partitioned into soil evaporation and canopy transpiration by partitioning available energy A using vegetation cover fraction F_c. Available energy components for canopy (A_{canopy}) and soil (A_{soil}) surface were generated using:

$$A_{canopy} = F_c \times A$$
(13)

$$A_{soil} = (1 - F_c) \times A$$
(14)

where A is approximated as net radiation R_n consisting both net shortwave radiation and net longwave radiation as soil heat flux is nearly zero in daily scale, and F_c was estimated from remote sensed LAI data.

The Penman-Monteith equation was used to generate vegetation transpiration as:

$$\lambda E_{canopy} = \frac{\Delta A_{canopy} + \rho C_p VPD g_a}{\Delta + \gamma(1 + g_a / g_c)}$$
(15)

where λE_{canopy} (W m^{-2}) is the latent heat flux of canopy, Δ (Pa K^{-1}) is the slope of the curve relating saturated water vapor pressure e_{sat} (Pa) to air temperature T (K), ρ (kg m^{-3}) is air density, C_p (J kg^{-1} K^{-1}) is the specific heat of air at constant pressure, VPD (Pa) is the vapor pressure deficit of air, g_a (m s^{-1}) is aerodynamic conductance, γ (Pa k^{-1}) is psychometric constant, and g_c (m s^{-1}) is canopy conductance.

The canopy conductance g_c, is influenced by g_{sx} (maximum stomatal conductance of leaves at the top of canopy), LAI, absorbed shortwave radiation, and VPD, which can be described as:

$$g_c = \frac{g_{sx}}{K_Q} \ln\left[\frac{Q_h + Q_{50}}{Q_h \exp(-K_Q LAI) + Q_{50}}\right]\left[\frac{1}{1 + VPD/D_{50}}\right]$$
(16)

where K_Q is the extinction coefficient for photosynthetically active radiation, Q_h is the photosynthetically active radiation at the top of canopy, Q_{50} and D_{50} are the values of absorbed photosynthetically active radiation and water vapor deficit when stomatal conductance is half its maximum value, respectively. K_Q, Q_{50}, and D_{50} were assigned to 0.6, 2.6 MJ m^{-2} d^{-1} and 800 Pa, respectively (Zhang *et al.*, 2008). Values of g_a and g_{sx} were considered as biome specific and assigned constant values for different vegetation types by referring to Zhang *et al.* (2008).

Soil evaporation was calculated using a soil evaporation equation described in Zhang *et al.* (2009)

and Mu *et al.* (2010), which is described as:

$$\lambda E_{\text{soil}} = RH^{(VPD/k)} \frac{\Delta A_{\text{soil}} + \rho C_{\text{p}} VPDg_{\text{a}}}{\Delta + \gamma \times g_{\text{a}} / g_{\text{totc}}} \tag{17}$$

where λE_{soil} (W m^{-2}) is the latent heat flux of soil, RH is the relative humidity of air with values ranging from 0 to 1, k (Pa) is a parameter to fit the complementary relationship and is empirically adjusted for different vegetation types, and g_{totc} (m s^{-1}) is the corrected value of total aerodynamic conductance as described by Zhang *et al.* (2010).

Potential evapotranspiration, E_{p}, was calculated using the Priestley and Taylor equation (Priestley and Taylor, 1972):

$$\lambda E_{\text{p}} = \varphi A \frac{\Delta}{\Delta + \gamma} \tag{18}$$

where the Priestley-Taylor coefficient φ was set to 1.26 following Priestley and Taylor (1972).

Table 1. The parameter values of the different vegetation types.

Vegetation type	LUE_{max}^{su} (gC/MJ)	LUE_{max}^{sh} (gC/MJ)	T_{opt} (°C)
CRO	1.114	2.913	26
CSH	0.552	2.446	20
DBF	0.680	3.030	20
DNF	0.403	1.700	15
EBF	0.706	3.079	25
ENF	0.678	3.020	15
GRA	0.603	2.833	18
MF	0.795	2.917	17
OSH	0.366	1.807	16
SAV	0.615	2.914	20
WET	0.603	2.833	18
WSAV	0.562	2.810	19

3. Input Data

The input data include remote sensing data, meteorology data, elevation data and land cover data, which are listed in Table 2.

Table 2. The data used in the algorithm of GPP and NPP estimation

Data Name	Unit	Temporal resolution	Spatial resolution	Data Source
FPAR	——	8d	0.05°	GLASS
LAI	m²/m²	8d	0.05°	GLASS
temperature	K	12h	0.75°	ERA-Interim
dewpoint temperature	K	12h	0.75°	ERA-Interim
Surface net solar radiation	MJ/m²	12h	0.75°	ERA-Interim

Surface net thermal radiation	MJ/m^2	12h	0.75°	ERA-Interim
Surface solar radiation downwards	MJ/m^2	12h	0.75°	ERA-Interim
Land cover product	——	1yr	0.05°	MCD12C1
DEM	km		1km	GLOBE

3.1 GLASS LAI and FPAR Products

The Global Change Data Processing and Analysis Center of Beijing Normal University generated and published the GLASS product set (Liang et al., 2013), and LAI and FPAR are two products in the GLASS product set. The GLASS LAI products include two categories. The GLASS MODIS product was calculated from MODIS surface reflectance data, and the GLASS MODIS LAI product, which includes data from 2000 to 2015, was provided in a sinusoidal projection at a spatial resolution of 1 km and a temporal resolution of 8 days. The other dataset was derived from the Long-Term Data Record (LTDR) of the Advanced Very High Resolution Radiometer (AVHRR) reflectance data (GLASS AVHRR). The latest version of the GLASS AVHRR LAI product, which includes data from 1981 to 2018, was provided in a geographic latitude/longitude projection at a spatial resolution of 0.05° and a temporal resolution of 8 days. The latest version of the GLASS AVHRR LAI product was used in this study (http://www.glass.umd.edu/LAI/AVHRR/). The comparison of the GLASS AVHRR LAI products against the LAI values derived from the high-resolution reference maps demonstrated that the GLASS AVHRR LAI values were more accurate than the National Centers for Environmental Information (NCEI) AVHRR LAI, the Global Inventory Monitoring and Modeling System (GIMMS3g) LAI and the Long-term Global Mapping (GLOBMAP) LAI values (Xiao et al., 2017).

The GLASS AVHRR FPAR product was calculated from GLASS AVHRR LAI products (http://www.glass.umd.edu/FAPAR/AVHRR/), and it has the same spatial and temporal resolution as the GLASS AVHRR LAI product. A comparison of the GLASS AVHRR FPAR and the other FPAR values derived from high-resolution reference maps demonstrated that the GLASS AVHRR FPAR product provided a better performance than the NCEI AVHRR FPAR product and the GIMMS3g FPAR product (Xiao et al., 2018).

3.2 MODIS Land Cover Product

The combined Terra and Aqua MODIS Land Cover Climate Modeling Grid (MCD12C1) Version 6 data product adopts the same algorithm as the land cover type (MCD12Q1) Version 6 data product and provides a spatially aggregated and reprojected version, which can be downloaded from https://e4ftl01.cr.usgs.gov/MOTA/MCD12C1.006/ (Damien et al., 2018). It contains three classification schemes: that of the International Geosphere-Biosphere Programme (IGBP), that of the University of Maryland (UMD), and the leaf area index (LAI).The IGBP classification product from 2001 to 2018 was used to produce global GPP and NPP products, which provides 17 land cover classifications with an annual interval and a spatial resolution of 0.05°, and we used the product in 2001 as a replacement for the period from 1981-2000 since there was no product for before 2001 (Figure 2).
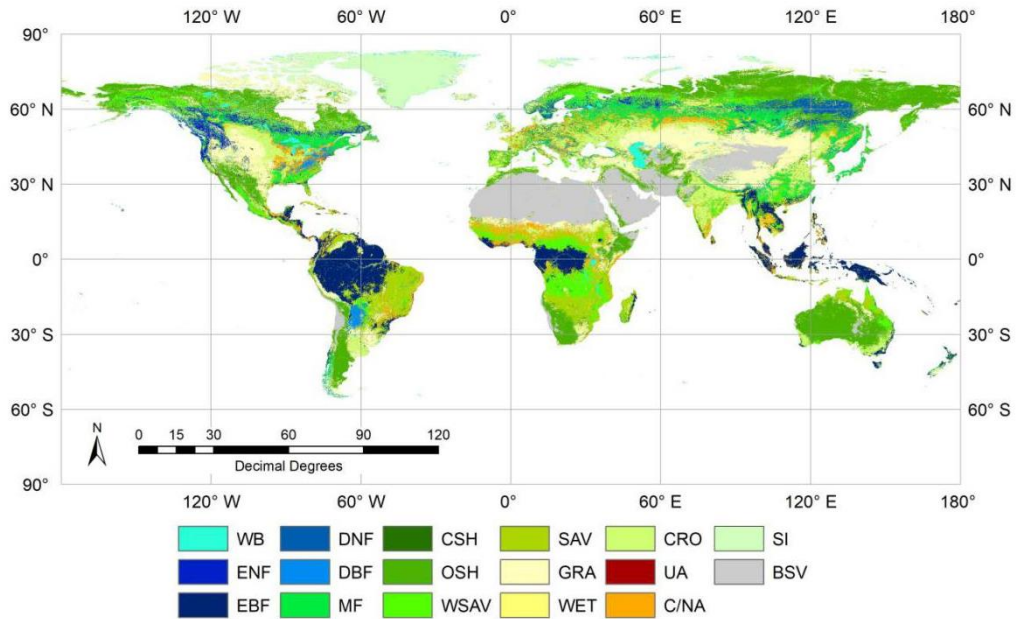
Figure 2. The global land cover map of the IGBP classification schemes. The full name of each land cover type is as follows: EBF: evergreen broadleaf forest; DBF: deciduous broadleaf forest; ENF: evergreen needleleaf forest; DNF: deciduous needleleaf forest; MF: mixed forest; CSH: closed shrubland; OSH: open shrublands; WSAV: woody savanna; SAV: savanna; GRA: grassland; WET: permanent wetland; CRO: cropland; UA: urban area; C/NV: cropland-natural vegetation mosaic; SI: snow and ice; BSV: barren or sparsely vegetated.

3.3 Meteorological Data

The ERA-Interim product was used as the meteorological input data. It is the global atmospheric reanalysis data generated by the European Centre for Medium-Range Weather Forecasts (ECMWF) from 1979 to 2019 and can be downloaded from https://apps.ecmwf.int/datasets/data/interim-full-daily/levtype=sfc/ (Berrisford et al., 2011). In our research, the daily dewpoint temperature and air temperature, surface net solar radiation, surface net thermal radiation, and surface solar radiation downward were obtained by averaging the 12 hour data. A bilinear interpolation was used to produce the 0.05° data since the spatial resolution of these data was 0.75°, and the effect of altitude was also taken into account in the interpolation of temperature. The relative humidity was calculated from the dewpoint temperature and temperature.

3.4 DEM Data

The DEM data were derived from the Global Land One-Kilometer Base Elevation (GLOBE) Version 1.0 (http://www.ngdc.noaa.gov/mgg/topo/globe.html). The GLOBE DEM is a global dataset covering from 180° west to 180° east longitude and 90° north to 90° south latitude; the spatial resolution of these data was 1 km (Hastings and Dunbar, 1999), and the data were aggregated to the spatial resolution of 0.05°.

4. Output Data

The output data was global GPP and NPP products from 1981 to 2018. The detail information of the products is as below:

Name: 5-km global GPP and NPP products

Period: 1981-2018

Projection: geographic latitude/longitude;

Spatial resolution: 0.05°;

Temporal resolution: 8 days;

Data format: Tiff;

Data type: integer (16bit);

Upper left coordinates: -180°E, 90°N;

Scale factor: 100;

Unit: $gCm^{-2}d^{-1}$.

5. Preliminary validation

To evaluate the MuSyQ GPP product, we downloaded the FLUXNET2015 dataset (https://FLUXNET.fluxdata.org/). This dataset includes observation data of the carbon flux and other climate data from 2003 to 2014 from 212 global FLUXNET sites.

We extracted the FLUXNET GPP data for those sites where the land cover types matched the MCD12C1 data and compared the FLUXNET GPP with the MuSyQ GPP. The results showed that R^2 is 0.559 and root mean square error (RMSE) is 2.782 gC/m^2d (Figure 3). However, there was a large-scale difference between the *in situ* GPP observations and the 0.05 degree remote sensing data. The GPP observation source area ranged from tens of meters to several kilometers, which varied with changes in instrument height, wind direction and wind speed. At the same time, the internal heterogeneity of pixels in 5 km remote sensing data is large, which leads to many mixed pixels. The inconsistency between the scale of the remote sensing pixel and the *in situ* GPP observation inevitably leads to uncertainty in the validation results.
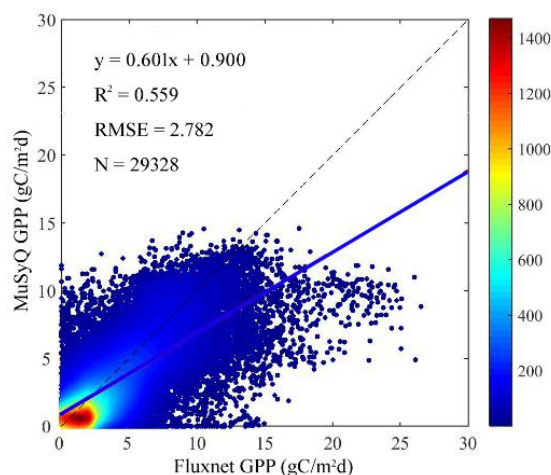

Figure 3. The comparison between MuSyQ GPP and FLUXNET GPP

Acknowledgements

References

Berrisford, P.; Dee, D.; Poli, P.; Brugge, R.; Fielding, K.; Fuentes, M.; Kallberg,P.; Kobayashi, S.; Uppala, S. ; Simmons, A. The ERA-Interim archive Version 2.0. 2011.

Cui, T.X.; Wang ,Y.J.; Sun, R.; Qiao, C.; Fan, W.; Jiang, G.; Hao, L.; Zhang, L. Estimating vegetation primary production in the Heihe River Basin of China with multi-source and multi-scale data. PLoS ONE. 2016, 11(4): e0153971.

Damien, S.M.; Mark, A.F. User Guide to Collection 6 MODIS Land Cover (MCD12Q1 and MCD12C1) Product. 2018.

Duan, Q.Y.; Sorooshian, S.; Gupta, V. Effective and efficient global optimization for conceptual rainfall-runoff models. Water resources research. 1992, 28, 1015-1031.

Hastings, D.; P.K. Dunbar. Global Land One-kilometer Base Elevation (GLOBE) v.1. National Geophysical Data Center, NOAA. 1999.

He, M.Z.; Ju, W.M.; Zhou, Y.L.; Chen, J.M.; He, H.L.; Wang, S.Q.; Wang, H.M.; Guan, D.X.; Yan, J.H.; Li, Y.N.; et al. Development of a two-leaf light use efficiency model for improving the calculation of terrestrial gross primary productivity. Agricultural and Forest Meteorology. 2013, 173, 28–39.

Liang, S.L. ; Zhao, X. ; Liu, S.H; et al. A long-term Global LAnd Surface Satellite (GLASS) data-set for environmental studies. International Journal of Digital Earth. 2013, 6(sup1), 5-33.

Lieth, H. Modeling the primary productivity of the world. In Primary Productivity of the Biosphere; Springer: Berlin/ Heidelberg, Germany, 1975; pp. 237–263.

Liu, J.; Chen, J.M.; Cihlar, J.; Park, W.M. A process-based boreal ecosystem productivity simulator using remote sensing inputs.Remote Sensing of Environment. 1997, 62, 158-175.

McGuire, A. D. ; Melillo, J. M. ; Kicklighter, D. W. ; Joyce, L. A. Equilibrium responses of soil carbon to climate change: Empirical and process-based estimates. Journal of Biogeography. 1996, 22, 785-796.

Mu, Q.Z.; Zhao, M.S.; Running, S.W. Improvements to a MODIS global terrestrial evapotranspiration algorithm. Remote Sens. Environ. 2011, 115, 1781-1800.

Potter, C. S. ; Randerson, J. T. ; Field, C. B. ; Matson, P. A. ; Vitousek, P. M. ; Mooney, H. A. ; Klooster, S. A. Terrestrial ecosystem production:A process model based on global satellite and surface data. Glob. Biogeochem. Cycles. 1993. 7, 811-841.

Priestley, C. H. B. ; Taylor, R. J. On the assessment of surface heat flux and evaporation using large-scale parameters. Mon. Weather Rev. 1972. 100, 81–92.

Prince, S. D. ; Goward, S. N. Global primary production:A remote sensing approach. J. Biogeogr. 1995. 22, 815-835.

Running, S.W.; Hunt, Jr., E. Raymond. Generalization of a forest ecosystem process model for other biomes,BIOME-BCG, and an application for global-scale models. In Scaling Physiological Processes. Academic Press:San Diego, CA, USA, 1993, 141-158.

Uchijima, Z.; Seino, H. Agroclimatic evaluation of net primary productivity of natural vegetations. J. Agric. Meteorol. 1985, 40, 343–352.

Wang, M.J.; Sun, R.; Zhu, A.R.; Xiao, Z. Q. Evaluation and Comparison of Light Use Efficiency and Gross Primary Productivity Using Three Different Approaches. Remote Sensing. 2020, 12, 1003.

Xiao, X.M.; Hollinger, D.; Aber, J.; Goltz, M.; A.Davidson, Eric.; Zhang, Q.Y.; Moore III, B. Satellite-based modeling of gross primary production in an evergreen needleleaf forest. Remote

sensing of environment. 2004, 89, 519-534.

Xiao, Z.Q.; Liang, S.L.; Jiang, B. Evaluation of four long time-series global leaf area index products. Agricultural and Forest Meteorology. 2017, 246, 218-230.

Xiao, Z.Q.; Liang, S.L.; Sun, R. Evaluation of three long time series for global Fraction of Absorbed Photosynthetically Active Radiation (FAPAR) products. IEEE Transactions on Geoscience and Remote Sensing. 2018, 56: 5509-5524.

Xin, Q.C.; Gong, P.; Suyker, A.E.; Si, Y.L. Effects of the partitioning of diffuse and direct solar radiation on satellite-based modeling of crop gross primary production. International Journal of Applied Earth Observation and Geoinformation. 2016, 50, 51–63.

Yu, T.; Sun, R.; Xiao, Z.Q. ;Zhang , Q.; Liu, G.; Cui, T.X.; Wang, J.M. Estimation of Global Vegetation Productivity from Global LAnd Surface Satellite Data. Remote sensing. 2018, 10, 327.

Yuan, W.P.; Liu, S.G.; Zhou, G.S.; Zhou, G.Y.; Tieszen, L.L.; Baldocchi, D.; Bernhofer, C. et al. Deriving a light use efficiency model from eddy covariance flux data for predicting daily gross primary production across biomes. Agricultural and Forest Meteorology. 2007, 143, 189-207.

Zhang, K.; Kimball, J.S.; Mu, Q.; Jones, L.A.; Goetz, S.J.; Running, S.W. Satellite based analysis of northern ET trends and associated changes in the regional water balance from 1983 to 2005. Journal of Hydrology. 2009, 379,92-110.

Zhang, K.; Kimball, J.S.; Nemani, R.R.; Running, S.W. A continuous satellite-derived global record of land surface evapotranspiration from 1983 to 2006. Water Resour. Res. 2010, 46.

Zhang, Y.Q.; Chiew, F.H.S.; Zhang, L.; Leuning, R.; Cleugh, H.A. Estimating catchment evaporation and runoff using MODIS leaf area index and the penman-monteith equation. Water Resour. Res. 2008, 44.

Zhao, M.S.; Running, S.W. Drought-induced reduction in global terrestrial net primary production from 2000 through 2009. Science. 2010, 329, 940-943.

Citation

Wang, M.J.; Sun, R.; Zhu, A.R.; Xiao, Z. Q. Evaluation and Comparison of Light Use Efficiency and Gross Primary Productivity Using Three Different Approaches. Remote Sensing. 2020, 12, 1003.

Yu, T.; Sun, R.; Xiao, Z.Q. ;Zhang , Q.; Liu, G.; Cui, T.X.; Wang, J.M. Estimation of Global Vegetation Productivity from Global LAnd Surface Satellite Data. Remote sensing. 2018, 10, 327.

Cui, T.X.; Wang ,Y.J.; Sun, R.; Qiao, C.; Fan, W.; Jiang, G.; Hao, L.; Zhang, L. Estimating vegetation primary production in the Heihe River Basin of China with multi-source and multi-scale data. PLoS ONE. 2016, 11(4): e0153971.